A Novel Lithium-ion Battery Pack Modeling Framework - Series-Connected Case Study

Trey Weaver[1], Anirudh Allam[2], and Simona Onori[2,*] *IEEE Senior Member*

***Abstract*— In this paper, a novel physics-based modeling framework is developed for lithium ion battery packs. To address a gap in the literature for pack-level simulation, we establish a high fidelity physics-based model that incorporates electrochemical-thermal-aging behavior for each cell and which is then upscaled at the pack level by incorporating electrical and thermal interaction terms. Such a construct is suitable both for performance analysis upon cell heterogeneity as well as control and optimization for on-board operation. Governing equations in the form of Partial Differential Equations (PDEs) are discretized into a system of Ordinary Differential Equations (ODEs) using Finite Difference and Finite Volume methods and reformulated into state-space models for both cell and pack dynamics. Computational time studies are conducted to demonstrate the effects of spatial discretization fidelity and pack size on simulation time. Pack model predictive capabilities are exercised by inducing hetereogeinity in the cell design parameters and effects of parameter perturbation are shown for pack voltage and energy responses. The goal for this modeling framework is to provide a computationally-feasible and easily scalable platform for high-fidelity offline simulation and optimization without compromising the integrity of cell dynamics across multiple time scales.**

I. INTRODUCTION

Despite the broad literature covering physics-based approaches for lithium-ion battery (LIB) modeling applications, there is a current gap addressing battery pack-level applications. To date, there has been limited use of computationally-tractable models for pack-level control and optimization purposes that simultaneously consider electrochemical, thermal and aging cell dynamics, as well as cell-to-cell thermal interactions, from physics-based perspectives. A fundamental challenge of battery pack modeling is that pack-level performance cannot be accurately extrapolated from single-cell models. This is due not only to manufacturing variations between cells and non-uniform degradation rates, but to the very fact of the cells being connected in series or parallel within the pack. As shown in [1], battery pack aging dynamics can be understood through the phenomena of thermal retroactivity, whereby the state-of-health of an individual cell is affected by the aging state of upstream and downstream cells through their interconnected thermal behaviors. This divergence between cell and pack aging behavior has been demonstrated in experimental studies, with particular focus given to elevated and non-uniform temperatures accelerating pack degradation [2] and manufacturing variances between cells limiting pack capacity [3]. Given this complex interplay, we believe that detailed consideration of aging, cell-to-cell interactions and cell heterogeneity is an important step in the development of robust battery management system (BMS) design. For single-cell control and optimization, aging-conscious modeling frameworks have been explored in the literature across a broad span of complexities, ranging from Equivalent Circuit Model (ECM) with semi-empirical capacity fade relationship [4] to pseudo two-dimensional (P2D) electrochemical-thermal models with simplified Solid Electrolyte Interphase (SEI) growth [5]. For pack-level control and optimization, the majority of studies have tended towards simplified or reduced-order modeling approaches. The most common approach is to integrate series-or parallel-connected ECMs with simple thermal models (e.g. lumped capacitance) and semi-empirical aging relationships [6], [7]. Others implement physics-based models for a subset of cell dynamics, but simplify or neglect important contributions such as aging, thermal interconnections or cell heterogeneity [8],[9]. Some approaches have included physics-based electrochemical-thermal-aging models but scaled up the pack response from a reference cell using a Taylor approximation sensitivity equation and left out thermal interactions between cells [10]. From the literature review, it follows that a comprehensive model that can closely predict the electrochemical, thermal, and aging behavior at the pack-level by accounting for thermal interactions in between cells is lacking. To that end, the primary objective of this paper is to propose a state-space modeling framework for a battery pack that gives detailed consideration of relevant dynamics while remaining computationally-feasible and easily scalable, with the ultimate goal of implementation in high-fidelity offline simulation and optimization applications. The novel contributions of this paper are: 1a) the state-space formulation of cell level electrochemical, thermal and aging dynamics, and 1b) their use in the pack level dynamics modeling after being augmented with cell-to-cell interconnection relations, 2) computational time assessment and cell-level hetereogeity study for pack level performance in terms of voltage and energy of a series-connected module.

II. CELL GOVERNING EQUATIONS

For this work, each Li-ion cell is modeled with coupled nonlinear PDEs, ODEs and differential algebraic equations (DAEs) describing the electrochemical, thermal and aging dynamics. Electroltye enhanced single particle model (ESPM) framework is applied to simplify the first-principles approach adopted in the P2D model [15]. We restrict our discussion to 1-dimensional battery packs of N_{cells} cells

[1]T. Weaver is with the Chemical Engineering Department, [2]A. Allam and S. Onori are with the Energy Resources Engineering Department, Stanford University, Stanford, CA 94305, USA (email: (weaverwe, aallam, sonori)@stanford.edu) *S. Onori is the corresponding author.

TABLE I: Electrochemical-thermal-aging dynamics of a LIB cell

Electrochemical dynamics [11]		
Mass conservation in solid phase	$\frac{\partial c_{s,j}}{\partial t} = \frac{D_{s,j}}{r^2}\frac{\partial}{\partial r}\left[r^2\frac{\partial c_{s,j}}{\partial r}\right], \quad j \in [n,p]$ $\left.\frac{\partial c_{s,j}}{\partial r}\right\|_{r=0} = 0 \quad \left.\frac{\partial c_{s,j}}{\partial r}\right\|_{r=R_{s,j}} = \frac{\pm I_{App}}{D_{s,j}a_{s,j}AL_jF} - g_{s,j}(C_{s,j}^{surf}, C_{solv}^{surf}, T_c, I_{app}, L_{sei})$	(1)
Mass conservation in electrolyte phase	$\epsilon_e\frac{\partial c_e}{\partial t} = \frac{\partial}{\partial x}\left(D_e^{eff}\frac{\partial c_e}{\partial x}\right) + \left(1-t_0^+\right)\frac{g_{e,j}I_{App}}{AL_jF}, \quad j \in [n,s,p]$ $\left.\frac{\partial c_e}{\partial x}\right\|_{x=0} = \left.\frac{\partial c_e}{\partial x}\right\|_{x=L_n+L_s+L_p} = 0$ $D_{e,n}^{eff}(c_{e,n},T)\left(\frac{\partial c_{e,n}}{\partial x}(x,t)\right)\Big\|_{x=L_n} = D_{e,s}^{eff}(c_{e,s},T)\left(\frac{\partial c_{e,s}}{\partial x}(x,t)\right)\Big\|_{x=L_n}$ $D_{e,s}^{eff}(c_{e,s},T)\left(\frac{\partial c_{e,s}}{\partial x}(x,t)\right)\Big\|_{x=L_n+L_s} = D_{e,p}^{eff}(c_{e,p},T)\left(\frac{\partial c_{e,s}}{\partial x}(x,t)\right)\Big\|_{x=L_n+L_s}$	(2)
Charge conservation in electrolyte phase	$\kappa_e^{eff}\frac{\partial^2\phi_e}{\partial x^2} - \kappa_D^{eff}\frac{\partial^2 \ln c_e}{\partial x^2} + \frac{I_{app}}{a_{s,n}AL_j} = 0, \quad j \in [n,s,p]$ $\left.\frac{\partial \Phi_e}{\partial x}\right\|_{x=0} = \left.\frac{\partial \Phi_e}{\partial x}\right\|_{x=L_n+L_s+L_p} = 0$	(3)
Electrode Overpotential	$\eta_j = \frac{R_gT_c}{0.5F}sinh^{-1}\left(\frac{I_{app}}{2Aa_{s,j}L_ji_{0,j}}\right), \quad j \in [n,p]$	(4)
Exchange Current Density	$i_{0,j} = k_j\sqrt{c_{e,j}^{avg}c_{s,j}^{surf}\left(c_{s,j}^{max}-c_{s,j}^{surf}\right)}, \quad j \in [n,p]$	(5)
Cell voltage	$V_{cell} = U_p + \eta_p - U_n - \eta_n + \Delta\Phi_e - I_{app}(R_l + R_{el} + R_{sei})$	(6)
Thermal dynamics [12]		
Cell Core Heat Balance	$C_c\frac{dT_c}{dt} = I_{app}(V_{oc} - V_{cell}) + \frac{T_s - T_c}{R_c}$	(7)
Cell Surface Heat Balance	$C_s\frac{dT_s}{dt} = \frac{T_{amb} - T_s}{R_u} - \frac{T_s - T_c}{R_c}$	(8)
Aging dynamics [13], [14]		
Mass conservation in SEI	$\frac{\partial c_{solv}}{\partial t} = D_{solv}\frac{\partial^2 c_{solv}}{\partial r^2} - \frac{dL_{sei}}{dt}\frac{\partial c_{solv}}{\partial r},$ $-D_{solv}\left.\frac{\partial c_{solv}}{\partial r}\right\|_{r=R_{s,n}} + \frac{dL_{sei}}{dt}c_{solv}^{surf} = \frac{i_s}{F}$ $\left.c_{solv}\right\|_{r=R_n+L_{sei}} = \epsilon_{sei}C_{solv}^{bulk}$	(9)
SEI layer growth	$\frac{dL_{sei}}{dt} = -\frac{i_sM_{sei}}{2F\rho_{sei}},$	(10)
Side reaction current density	$i_s = -2Fk_f(c_{s,n}^{surf})^2c_{solv}^{surf}\exp\left[\frac{-\beta F}{R_gT_c}(\Phi_{s,n} - R_{sei}I_{app} - U_s)\right]$	(11)
Cell capacity loss	$\frac{dQ}{dt} = i_sAL_na_{s,n}$	(12)

connected in series. Throughout, the subscript i refers to the discretization grid position when converting from PDEs to ODEs in solid electrode, electrolyte and SEI layer spatial dimensions; the subscript j, where $j \in [n,s,p]$, refers to the cell domain (e.g. n = anode, s = separator, p = cathode); and superscript k refers to the cell position within the pack.

A. Electrochemical Governing and Response Equations

ESPM approximates the electrode active material as single spherical particles with uniform current density. The model is described by three governing PDEs for electrochemical dynamics given by (1), (2), and (3) in Table I, respectively. Further, surface overpotentials, η_j, given in (4), are calculated assuming Butler-Volmer kinetics for the electrode intercalation reaction using electrode surface and averaged electrolyte concentration for each domain, whereas the exchange current density, for each electrode, $i_{0,j}$, is described by (5). Given the concentration and potential distribution in the electrodes and electrolyte, cell voltage can be calculated by (6). Open-circuit potentials of electrodes, U_j, are calculated from empirical relationships based on electrode surface concentration stoichiometry [16]. Cell ohmic resistance is separated into three terms, R_l, R_{el}, R_{sei}, representing lumped contact, electrolyte, and SEI layer resistances. Electrolyte and SEI resistances are given by [14]

$$R_{el} = \frac{1}{2A}\left[\frac{L_n}{\kappa_{e,n}^{eff}} + \frac{2L_s}{\kappa_{e,s}^{eff}} + \frac{L_p}{\kappa_{e,p}^{eff}}\right], \tag{13}$$

$$R_{sei} = \frac{L_{sei}}{a_{s,n}AL_n\kappa_{sei}}, \tag{14}$$

where $\kappa_{e,j}^{eff} = f\left(c_{e,j}^{avg}, \epsilon_{e,j}\right)$.

B. Two-State Thermal Model

Thermal dynamics are modeled using a lumped parameter two-state thermal model that considers core, T_c, and surface, T_s, temperatures of each cell [12], as expressed in (7) and (8). Heat generation in the battery cells is attributed to electrode overpotential and Joule heating; entropic contributions are

assumed to be negligible. To account for cell-to-cell heat transfer at the pack-level, (8) is modified as follows:

$$C_s \frac{dT_s^{Cell\,k}}{dt} = \frac{T_{amb} - T_s^{Cell\,k}}{R_u} - \frac{T_s^{Cell\,k} - T_c^{Cell\,k}}{R_c} + \frac{T_s^{Cell\,k} - T_s^{Cell\,k+1}}{R_m} + \frac{T_s^{Cell\,k} - T_s^{Cell\,k-1}}{R_m}. \quad (15)$$

Cell-to-cell heat transfer is a primary interconnection that differentiates battery pack-level aging dynamics from cell-level and is therefore a critical consideration for pack-level modeling frameworks[1].

C. Aging Dynamics - Solvent Diffusion and Side-Reaction

We adopt a physics-based approach for battery aging that considers anode SEI layer growth as a function of both solvent reduction kinetics and diffusion dynamics across the growing SEI layer in order to predict cell capacity loss and power fade [13], [14]. The solvent concentration available for reduction reaction at the anode surface is modeled by (9). The SEI layer growth can be modeled as linearly related to side-reaction current by (10), where the side reaction current is given by (11). Capacity loss is attributed to lithium content consumed by solvent reduction, estimated by integrating side reaction current across the anode active surface area (12). Anode porosity, $\epsilon_{e,n}$, is updated based on the growing SEI layer thickness using a volume balance approach [14] given by $\epsilon_{e,n} = 1 - \epsilon_{s,n}\left(1 + \frac{3L_{sei}}{R_{s,n}}\right) - \epsilon_{f,n}$.

D. State-dependent Parameters

To ensure the most robust model performance, concentration- and temperature-dependent transport and kinetic parameters are updated based on the relevant state variables at each time-point. Solid electrode parameters, such as $D_{s,j}$ and k_j, follow an Arrhenius relationship with temperature as given in [15]. Empirical relationships for concentration and temperature dependencies of electrolyte parameters $D_{e,j}$ and $\kappa_{e,j}$ are taken from [17].

III. DISCRETIZATION METHODS

To solve the system of coupled electrochemical and aging dynamics, PDEs with spatial dependence (e.g. Solid, Electrolyte and SEI Layer Solvent Diffusion) are discretized using Finite Difference Method (FDM) and Finite Volume Method (FVM), as described below.

A. Finite Difference Method - Solid Phase

Solid electrode diffusion PDEs are discretized using FDM, with Central Difference schemes being applied for both 1^{st} and 2^{nd} spatial derivatives. Using this discretization scheme, (1) is simplified to the following algorithm for each grid-point $i \in [1, N_{r,j}]$ as

$$\frac{\partial c_{s,j,i}}{\partial t} = \frac{D_{s,j}}{\Delta r_j^2} \cdot \left[\left(1 + \frac{1}{i}\right) c_{s,j,i+1} - 2c_{s,j,i}\left(1 - \frac{1}{i}\right) c_{s,j,i-1}\right] \quad (16)$$

[1]We assume here that the battery pack has no thermal management system and therefore can only expel heat to the ambient surroundings. This is a useful simplification in that it gives the worst case scenario for pack aging performance and can therefore be used as a baseline for evaluating thermal management strategies.

where $\Delta r_j = \frac{R_{s,j}}{N_{r,j} - 1}$. The algorithm is modified for concentration states at the sphere center and surface using the relevant boundary conditions. FDM is well-suited for this implementation of the Solid Diffusion equation because the empirical relationship for the diffusion coefficient does not depend on concentration and therefore does not vary between electrode grid points (see discussion in following section).

B. Finite Volume Method - Electrolyte Phase

Electrolyte diffusion dynamics is discretized with FVM rather than FDM. The empirical relationship used for electrolyte diffusivity is dependent on both concentration and temperature, such that the coefficient varies throughout the region [17]. FVM has been found to be particularly robust to variable coefficients due to its mass-conserving properties [18] and is therefore a more appropriate discretization scheme. In FVM, the state of each discretized cell is treated as a volume-average. Fluxes into and out of a given cell are equal to the respective fluxes of adjacent cells, thus maintaining conservation of mass. The following ODE is obtained by integrating (2) across a discretized cell centered at x_i to find volume average and discretizing spatial derivative using a Central Difference scheme, where $\Delta x_j = \frac{L_j}{N_{x,j}}$:

$$\epsilon_{e,j} \frac{\partial c_{e,i}}{\partial t} = \frac{1}{\Delta x_j^2}\left[D_{e,i+1/2}^{eff}\left(c_{e,i+1} - c_{e,i}\right) + D_{e,i-1/2}^{eff}\left(c_{e,i} - c_{e,i-1}\right)\right] + \left(1 - t_0^+\right)\frac{g_{e,j} I_{app}}{A L_j F}, \quad (17)$$

where $g_{e,j} = \begin{cases} 1 & \text{if } j = n \\ 0 & \text{if } j = s \\ -1 & \text{if } j = p \end{cases}$.

This formula can be applied across the entire electrolyte region due to its explicit consideration of discontinuities in diffusivity and porosity at cell boundaries, such as those that occur at the electrode/separator interfaces. Defining $\Theta = \frac{\Delta x_{j,i}}{\Delta x_{j,i-1} + \Delta x_{j,i}}$, transport properties are calculated at intermediate grid-points $x_{i\pm1/2}$, using the harmonic mean:

$$D_{e,i\pm1/2}^{eff} = \frac{D_{e,i}^{eff} D_{e,i\pm1}^{eff}}{\Theta D_{e,i}^{eff} + (1 - \Theta) D_{e,i\pm1}^{eff}}. \quad (18)$$

C. Non-dimensional FDM - Solvent Diffusion

When discretizing the solvent diffusion equation (9), it is necessary to account for the changing SEI layer thickness, which results in a time-varying grid size. The PDE is spatially non-dimensionalized with the updated SEI layer thickness at each time-point, and following the same steps described in [19] gives the final expression as

$$\frac{dc_{solv,i}}{dt} = \frac{D_{solv}}{\left(L_{sei}\Delta\xi\right)^2}\left(c_{solv,i+1} - 2c_{solv,i} + c_{solv,i-1}\right) + \frac{\xi - 1}{2L_{sei}\Delta\xi}\frac{dL_{sei}}{dt}\left(c_{solv,i+1} - c_{solv,i-1}\right) \quad (19)$$

where $\xi = \dfrac{r - R_{s,n}}{L_{sei}}$ and $\Delta\xi = \dfrac{1}{N_{sei} - 1}$.

D. Approximation - Conservation of Charge

Rather than spatially discretizing and integrating the resulting ODEs, the Conservation of Charge equation (3) is analytically integrated and solved. This allows for the difference in electrostatic potential between current collectors to be solved for based on the electrolyte concentration distribution at each time point.

IV. CELL-LEVEL STATE-SPACE FORMULATION

Following discretization, the governing PDEs are reduced to a system of ODEs in addition to algebraic expressions for electrochemical model outputs. This system of equations is reformulated into a cell-level state-space form. This approach is highly modular and can be rapidly scaled-up or -down in terms of both discretization fidelity and pack size. See Table II for detailed definitions of coefficient matrices. Note that coefficient matrices are not explicitly assembled for solvent diffusion dynamics due to the complexities introduced by non-dimensionalization. Instead, solvent diffusion dynamics are calculated algorithmically for each state, as described in (28), and solved in a coupled manner with all remaining dynamics.

Solid Phase Diffusion - Given the vector of discretized electrode states

$$\boldsymbol{c}_{s,j} = \begin{bmatrix} c_{s,j,1} \\ c_{s,j,2} \\ \vdots \\ c_{s,j,N_{r,j}} \end{bmatrix}_{N_{r,j} \text{ x } 1} \qquad \boldsymbol{c}_{s,j} \in \mathbb{R}^{N_{r,j}},\ c_{s,j,N_{r,j}} = c_{s,j}^{surf} \tag{20}$$

then the electrodes' state-space system is given by

$$\dot{\boldsymbol{c}}_{s,j} = \alpha_{s,j} A_{s,j} \boldsymbol{c}_{s,j} + \beta_{s,j} B_{s,j} \left[\boldsymbol{u} - g_{s,j}\right], \tag{21}$$

where $\boldsymbol{u} = I_{app}$,

$$\alpha_{s,j} = \frac{D_{s,j}}{\Delta r_j^2},\ \beta_{s,j} = \begin{cases} \dfrac{1}{AL_j F a_{s,j} \Delta r_j} & \text{if } j = n \\ \dfrac{-1}{AL_j F a_{s,j} \Delta r_j} & \text{if } j = p \end{cases}, \tag{22}$$

and

$$g_{s,j}(c_{s,j}^{surf}, c_{solv}^{surf}, T_c, \boldsymbol{u}, L_{sei}) = \begin{cases} a_{s,n} L_n A i_s & \text{if } j = n \\ 0 & \text{if } j = p \end{cases}. \tag{23}$$

is an aging-related non-linear input term which depends on multiple states across all dynamics of a given cell.

Electrolyte Diffusion - For each domain j, given the vector of discretized electrolyte states

$$\boldsymbol{c}_{e,j} = \begin{bmatrix} c_{e,j,1} \\ c_{e,j,2} \\ \vdots \\ c_{s,j,N_{x,j}} \end{bmatrix}_{N_{x,j} \text{ x } 1} \qquad \boldsymbol{c}_{e,j} \in \mathbb{R}^{N_{x,j}} \tag{24}$$

then the state-space system for the electrolyte dynamics is given by

$$\dot{\boldsymbol{c}}_e = A_e \boldsymbol{c}_e + \beta_e B_e \boldsymbol{u},\ \text{where } \beta_e = \frac{\left(1 - t_0^+\right)}{AL_j F}, \tag{25}$$

$$\boldsymbol{c}_e = \begin{bmatrix} \boldsymbol{c_{e,n}} \\ \boldsymbol{c_{e,s}} \\ \boldsymbol{c_{e,p}} \end{bmatrix}_{N_{el} \text{ x } 1} \text{ and } N_{el} = \sum_j N_{x,j}$$

SEI Layer Growth- The scalar L_{sei} aging state is given by

$$\dot{L}_{sei} = \beta_{sei} g_{s,n} \tag{26}$$

$$\text{where } \beta_{sei} = \frac{-M_{sei}}{2F\rho_{sei} a_{s,n} L_n A}$$

and $g_{s,n}$ is given by (23).

Solvent Diffusion- Given the discretized solvent diffusion state vector

$$\boldsymbol{c}_{solv} = \begin{bmatrix} c_{solv,1} \\ c_{solv,2} \\ \vdots \\ c_{solv,N_{sei}} \end{bmatrix}_{N_{sei} \text{ x } 1} \qquad \boldsymbol{c}_{solv} \in \mathbb{R}^{N_{sei}},\ c_{solv,1} = c_{solv}^{surf} \tag{27}$$

then the solvent diffusion state-space system is written as

$$\dot{\boldsymbol{c}}_{solv} = f_{solv}\left(\boldsymbol{c}_{solv}, L_{sei}, g_{s,n}\right) \text{ such that} \tag{28}$$

$$\dot{\boldsymbol{c}}_{solv} = \begin{cases} 2\alpha_{solv}(c_{solv,2} - c_{solv,1}) + \\ \qquad \beta_{solv}\left(\dfrac{i_s}{F} - \dfrac{dL_{sei}}{dt} c_{solv,1}\right) \text{ if } i = 1 \\ \alpha_{solv}\left(c_{solv,i+1} - 2c_{solv,i} + c_{solv,i-1}\right) + \\ \qquad \gamma_{solv}\left(c_{solv,i+1} - c_{solv,i-1}\right) \text{ if } 1<\text{i}<N_{sei} \\ 0 \text{ if } i = N_{sei} \end{cases}$$

$$\text{with } \alpha_{solv} = \frac{D_{solv}}{\left(L_{sei}\Delta\xi\right)^2},\ \gamma_{solv} = \left(\frac{\xi - 1}{2L_{sei}\Delta\xi} \frac{dL_{sei}}{dt}\right),$$

$$\beta_{solv} = \left(\frac{2}{L_{sei}\Delta\xi} + \frac{1}{D_{solv}} \frac{dL_{sei}}{dt}\right).$$

The output voltage equation is written as

$$\begin{aligned} V_{cell} = & U_p(c_{s,p}^{surf}) + \eta_p(c_{s,p}^{surf}, c_{e,p}^{avg}, T_c, u) - U_n(c_{s,n}^{surf}) - \\ & \eta_n(c_{s,n}^{surf}, c_{e,n}^{avg}, T_c, u) + \Delta\Phi_e - \boldsymbol{u}\left(R_l + R_{el} + R_{sei}\right). \end{aligned} \tag{29}$$

V. PACK-LEVEL STATE-SPACE FORMULATION

State-space matrices for each cell can be compiled into block-diagonal matrices representing the solid and liquid concentration states, as well as the aging (e.g., SEI) and thermal dynamics of the battery pack, as seen in Table III. Solvent diffusion dynamics at the pack level, on the other hand, is expressed by the implicit nonlinear function F_{solv}^{pack}. State vectors and input variables for each cell can be similarly concatenated, allowing all states across the module to be calculated en masse. The critical pack-level feature is in the thermal dynamics, that introduce the direct interconnection between adjacent cells in the battery pack. As seen in Table III, A_{therm}^{pack} relates surface temperature states, T_s, for adjacent cells, thus representing cell-to-cell

TABLE II: State-Space Coefficient Matrices for Discretized Diffusion Governing Equations

Solid Electrode Diffusion Matrices

$$A_{s,j} = \begin{bmatrix} -2 & 2 & 0 & 0 & \dots & 0 & 0 \\ 1/2 & -2 & 3/2 & 0 & \dots & 0 & 0 \\ 0 & 2/3 & -2 & 4/3 & \dots & 0 & 0 \\ \vdots & \vdots & \vdots & \vdots & \ddots & \vdots & \vdots \\ 0 & 0 & 0 & 0 & \dots & 2 & -2 \end{bmatrix}_{N_{r,j} \text{ x } N_{r,j}} \qquad B_{s,j} = \begin{bmatrix} 0 \\ 0 \\ 0 \\ \vdots \\ \left(2 + \frac{2}{N_r - 1}\right) \end{bmatrix}_{N_{r,j} \text{ x } 1}$$

Electrolyte Diffusion Matrices

$$A_e = \begin{bmatrix} -D^{eff}_{e,1/2} & D^{eff}_{e,1/2} & 0 & \dots & 0 & 0 \\ D^{eff}_{e,1/2} & -\left(D^{eff}_{e,1/2} + D^{eff}_{e,3/2}\right) & D^{eff}_{e,3/2} & \dots & 0 & 0 \\ \vdots & \vdots & \vdots & \ddots & \vdots & \vdots \\ 0 & 0 & 0 & \dots & D^{eff}_{e,N_{el}-3/2} & -D^{eff}_{e,N_{el}-3/2} \end{bmatrix}_{N_{el} \text{ x } N_{el}} \qquad B_e = \begin{bmatrix} (1)_{N_{x,n} \text{ x } 1} \\ (0)_{N_{x,s} \text{ x } 1} \\ (-1)_{N_{x,p} \text{ x } 1} \end{bmatrix}$$

heat transfer. Pack-level dynamics for series-connected packs can be summarized in compact form as

$$\begin{cases} \dot{\boldsymbol{c}}^{pack}_{s,j} & = A^{pack}_{s,j} \boldsymbol{c}^{pack}_{s,j} + B^{pack}_{s,j} \boldsymbol{u} - G^{pack}_{s,j} \\ \dot{\boldsymbol{c}}^{pack}_{e} & = A^{pack}_{e} \boldsymbol{c}^{pack}_{e} + B^{pack}_{e} \boldsymbol{u} \\ \dot{\boldsymbol{c}}^{pack}_{solv} & = F^{pack}_{solv} \\ \dot{\boldsymbol{L}}^{pack}_{sei} & = G^{pack}_{sei} \\ \dot{\boldsymbol{T}}^{pack}_{states} & = A^{pack}_{therm} \boldsymbol{T}^{pack}_{states} + B^{pack}_{therm} \boldsymbol{u} + G^{pack}_{therm} T_{amb} \end{cases} \tag{30}$$

where

$$\begin{aligned} G^{pack}_{s,j} &= G^{pack}_{s,j}\left(c^{surf}_{s,j}, c^{surf}_{solv}, T_c, \boldsymbol{u}, L_{sei}\right), \\ F^{pack}_{solv} &= F^{pack}_{solv}\left(\boldsymbol{c}_{solv}, L_{sei}, g_{s,n}\right), \\ G^{pack}_{sei} &= G^{pack}_{sei}\left(c^{surf}_{s,j}, c^{surf}_{solv}, T_c, \boldsymbol{u}, L_{sei}\right). \end{aligned}$$

Note that the solvent diffusion dynamic term F^{pack}_{solv} is a nonlinear function of the states and input (through $g_{s,n}$) representing the algorithms described in (28) for each cell of the pack. It is also worth noting that matrix prefactors such as $\alpha_{s,j}$ and $\beta_{s,j}$ vary between cells due to cell heterogeneity of design parameters, as well as non-uniform aging and temperature distribution, and are therefore not factored out of the block diagonal matrices, as seen in Table III.

VI. SIMULATION RESULTS

Computational Time Study: In order to evaluate the computational feasibility of this modeling framework, a series of computational time studies were performed across a range of discretization for a series-connected battery module of variable sizes. Simulations were executed on an Intel i7-6700 CPU with 4 processor cores @ 3.40 GHz and 8 GB of RAM. Computational time was quantified using the built-in MATLAB function 'timeit.' Two scenarios were tested: discharge from SOC = 1 at constant 1C-rate for a fixed nominal duration of 3600 seconds, as well as a dynamic US06 Drive Cycle with a fixed duration of 2700 seconds. The independent variables for each simulation condition were: N_{cells}, $N_{r,n}+N_{r,p}$, and $N_{el}+N_{sei}$. The state-space system was solved using built-in MATLAB solver 'ode15s', which is well-suited for stiff differential equations such as those considered here. The 1C discharge and US06 cycles for lowest

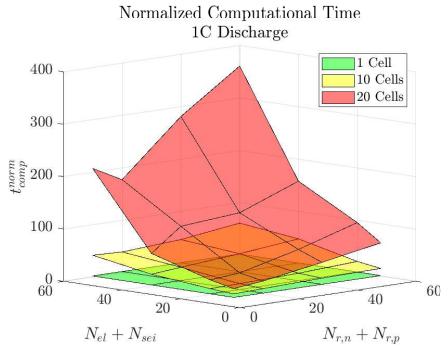

Fig. 1: Normalized computational time as a function of electrode and electrolyte discretization for packs of varying size

fidelity single cell took approximately 0.8 and 4.4 seconds, respectively, with US06 requiring additional computational time to meet ODE solver tolerances in response to the highly variable input, I_{app}. In Fig. 1, normalized computational time t^{norm}_{comp} is plotted, where t_{comp} at a given discretization and pack size is scaled by the lowest-fidelity single cell run time for 1C discharge scenario (obtained for $N_{cell} = 1$, $N_{r,n} = N_{r,p} = 5$, $N_{el} = 3+3+3$, $N_{sei} = 3$) as seen in the denominator of (31)

$$t^{norm}_{comp} = \frac{t_{comp}(N_{cells}, N_{r,n}+N_{r,p}, N_{el}+N_{sei})}{t_{comp}(1,10,12)\Big|_{Discharge}} \tag{31}$$

In terms of computational burden, changes in the number of electrolyte states were found to have a greater impact than equivalent magnitude changes in solid electrode states, as seen in the significantly greater slope of t^{comp}_{norm} against $N_{el}+N_{sei}$ than $N_{r,n}+N_{r,p}$ in Fig. 1. This could have important implications when optimizing discretization levels to balance model accuracy with expediency. Overall, computational time was found to increase at an exponential rate with total number of states in battery pack.

Parameter Sensitivity Analysis: To exercise the model's predictive capabilities and explore the impact of cell heterogeneity, we conducted parameter sensitivity analyses on pack-level performance for a 6-cell series-connected battery pack. In this study, battery design parameters related

TABLE III: Pack-level Block Diagonal Coefficient Matrices and Vectors

Solid Electrode Diffusion Matrices - Pack

$$A_{s,j}^{pack} = \begin{bmatrix} (\alpha_{s,j} A_{s,j})^{Cell\ 1} & & \\ & \ddots & \\ & & (\alpha_{s,j} A_{s,j})^{Cell\ N} \end{bmatrix}_{\substack{N_{cells} N_{r,j} \\ \times \\ N_{cells} N_{r,j}}} \quad B_{s,j}^{pack} = \begin{bmatrix} (\beta_{s,j} B_{s,j})^{Cell\ 1} \\ \vdots \\ (\beta_{s,j} B_{s,j})^{Cell\ N} \end{bmatrix}_{N_{cells} N_{r,j} \times 2} \quad \boldsymbol{c}_{s,j}^{pack} = \begin{bmatrix} \boldsymbol{c}_{s,j}^{Cell\ 1} \\ \vdots \\ \boldsymbol{c}_{s,j}^{Cell\ N} \end{bmatrix}$$

Electrolyte Diffusion Matrices - Pack

$$A_e^{pack} = \begin{bmatrix} A_e^{Cell\ 1} & & \\ & \cdots & \\ & & A_e^{Cell\ N} \end{bmatrix}_{\substack{N_{cells} N_{el} \\ \times \\ N_{cells} N_{el}}} \quad B_e^{pack} = \begin{bmatrix} (\beta_{e,j} B_{e,j})^{Cell\ 1} \\ \vdots \\ (\beta_{e,j} B_{e,j})^{Cell\ N} \end{bmatrix}_{N_{cells} N_{el} \times 2} \quad \boldsymbol{c}_e^{pack} = \begin{bmatrix} \boldsymbol{c}_e^{Cell\ 1} \\ \vdots \\ \boldsymbol{c}_e^{Cell\ N} \end{bmatrix}$$

Thermal State Matrices - Pack

$$A_{therm}^{pack} = \begin{bmatrix} \frac{-1}{R_c C_c} & \frac{1}{R_c C_c} & 0 & 0 & \cdots & 0 & 0 & 0 \\ \frac{1}{R_c C_s} & \frac{-1}{C_s}\left(\frac{1}{R_c}+\frac{1}{R_u}+\frac{1}{R_m}\right) & 0 & \frac{1}{R_m C_s} & \cdots & 0 & 0 & 0 \\ 0 & 0 & \frac{-1}{R_c C_c} & \frac{1}{R_c C_c} & \cdots & 0 & 0 & 0 \\ 0 & \frac{1}{R_m C_s} & \frac{1}{R_c C_s} & \frac{-1}{C_s}\left(\frac{1}{R_c}+\frac{1}{R_u}+\frac{2}{R_m}\right) & \cdots & 0 & 0 & 0 \\ \vdots & \vdots & \vdots & \vdots & \ddots & \vdots & \vdots & \vdots \\ 0 & 0 & 0 & 0 & \cdots & \frac{1}{R_m C_s} & \frac{1}{R_c C_s} & \frac{-1}{C_s}\left(\frac{1}{R_c}+\frac{1}{R_u}+\frac{1}{R_m}\right) \end{bmatrix}_{\substack{2N_{cells} \\ \times \\ 2N_{cells}}}$$

$$B_{therm}^{pack} = \begin{bmatrix} \frac{1}{C_c}\left(V_{oc} - V_{cell}\right)^{Cell\ 1} \\ 0 \\ \frac{1}{C_c}\left(V_{oc} - V_{cell}\right)^{Cell\ 2} \\ 0 \\ \vdots \\ 0 \end{bmatrix}_{2N_{cells} \times 1} \quad G_{therm}^{pack} = \begin{bmatrix} 0 \\ \frac{1}{R_u C_s} \\ 0 \\ \frac{1}{R_u C_s} \\ \vdots \\ \frac{1}{R_u C_s} \end{bmatrix}_{2N_{cells} \times 1} \quad \boldsymbol{T}_{states}^{pack} = \begin{bmatrix} T_c^{Cell\ 1} \\ T_s^{Cell\ 1} \\ T_c^{Cell\ 2} \\ T_s^{Cell\ 2} \\ \vdots \\ T_s^{Cell\ N} \end{bmatrix}_{2N_{cells} \times 1}$$

Aging Matrix & Nonlinear Input Matrices

$$\boldsymbol{L}_{sei}^{pack} = \begin{bmatrix} L_{sei}^{Cell\ 1} \\ \vdots \\ L_{sei}^{Cell\ N} \end{bmatrix}_{N_{cells} \times 1} \quad G_{s,j}^{pack} = \begin{bmatrix} [\beta_{s,j} B_{s,j} g_{s,j}]^{Cell\ 1} \\ \vdots \\ [\beta_{s,j} B_{s,j} g_{s,j}]^{Cell\ N} \end{bmatrix}_{N_{cells} N_{r,j} \times 1} \quad G_{sei}^{pack} = \begin{bmatrix} [\beta_{sei} g_{s,n}]^{Cell\ 1} \\ \vdots \\ [\beta_{sei} g_{s,n}]^{Cell\ N} \end{bmatrix}_{N_{cells} \times 1}$$

to cell geometry and transport/kinetic processes are considered, as listed on the x-axes of Figs. 2a and 2b, respectively. A single parameter was perturbed in each cell by a random value from uniform probability distribution $unif\left(-10\%, 10\%\right)$ of the nominal value for geometrical parameters or $unif\left(-80\%, 80\%\right)$ for transport/kinetic parameters[2], such that all cells had different values of the targeted parameter. All other parameters were held at nominal value, as identified in [20]. The perturbed pack was simulated for a 1C discharge cycle, producing $V_{pack,\theta}(t) = \sum_{k=1}^{N_{cells}} V_{cell,\theta}^{Cell\ k}$ where θ represents the perturbed parameter as listed in Figs. 2a and 2b. This procedure of random perturbation and simulation was repeated 100 times for each parameter in order to widely explore the possible combinations of perturbation levels across the pack. Perturbed pack results were compared to an unperturbed pack (i.e. nominal parameter values for all cells) in terms of pack voltage, $V_{pack,ref}(t) = \sum_{k=1}^{N_{cells}} V_{cell,ref}^{Cell\ k}$ and energy, $E_{pack,ref}(t) = \int_0^t V_{pack,ref}(\tau) I_{app}(\tau) d\tau$. The $V_{\%RMS}$ is the percentage Root Mean Square (RMS) voltage change of perturbed voltage, $V_{pack,\theta}$, from the reference value, $V_{pack,ref}$,

$$V_{\%RMS} = \sqrt{\frac{1}{t_{end}} \int_0^{t_{end}} \left(V_{pack,\theta} - V_{pack,ref}\right)^2 dt} \frac{100 t_{end}}{\int_0^{t_{end}} V_{pack,ref} dt} \tag{32}$$

[2]Note that different perturbation levels were chosen for geometrical and transport/kinetic parameters such that pack-level outcomes would fall within a physically-meaningful range and on comparable orders of magnitude.

where t_{end} is the time at which the limiting cell in either pack reaches its cutoff voltage, and $\%\Delta E$ is the percentage energy change given as

$$\%\Delta E = \frac{E_{pack,\theta}\left(t_{end,\theta}\right) - E_{pack,ref}\left(t_{end,ref}\right)}{E_{pack,ref}\left(t_{end,ref}\right)} 100 \tag{33}$$

where $t_{end,ref}$ and $t_{end,\theta}$ are the simulation end times for the reference and perturbed cases, respectively.

Sensitivity analyses revealed that both the predicted pack voltage and energy during discharge were most sensitive to geometrical parameters such as $\epsilon_{s,n}, L_n,$ and A that affect electrode capacity, particularly at the anode, as seen in Fig. 2a. Likewise, for transport and kinetic parameters, perturbations in $D_{s,n}$and k_n result in the largest voltage and energy deviations during discharge, as seen in Fig. 2b. Throughout this section, average $\%$-perturbation refers to the sum of perturbation levels of each cell divided by the number of cells[3], while $\%$-perturbation range refers to the difference between maximum and minimum perturbation levels in a pack [4]. We notice significant asymmetries where positive

[3]$\left(\text{e.g. } \frac{3\% + 3\% + (-3\%)}{3} = +1\%\text{-average perturbation}\right)$

[4]e.g. $max\left[3\%, 3\%, (-3\%)\right] - min\left[3\%, 3\%, (-3\%)\right]$ = +6%-perturbation range)

average perturbations of geometrical parameters across pack result in greater $V_{\%RMS}$, while negative average perturbations result in greater $\%\Delta E$ magnitude. Transport/kinetic parameters, on the other hand, show a consistently higher magnitude response for negative average perturbations. We can gain insight into this behavior by analyzing the variation of pack voltage profiles seen in Fig. 3a for a case study of $\epsilon_{s,n}$ perturbations, with particular emphasis given to marked Cases A, B and C. From Fig. 3a, we can see that the capacity at which a pack reaches end-of-discharge conditions varies widely, and is strongly dependent on the direction of perturbation (i.e. negative/positive)[5]. Because of the series connection modeled here, the battery pack is limited by the lowest capacity component cell such that any large magnitude negative perturbations in cell capacity across the pack will have a significant and direct impact on pack performance. This can be seen in Fig. 3b, where large negative $\%\Delta E_{pack}$ is seen to be insensitive to average $\%$-perturbation but highly correlated with large $\%$-perturbation range (see Case A). Packs with a wide range of perturbation levels across cells are highly likely to have a cell with a large magnitude negative perturbation, which causes such a cell to limit overall pack performance. On the other hand, Cases B and C show that positive $\%\Delta E_{pack}$ tends to occur only for packs with high average $\%$-perturbation and narrow $\%$-perturbation ranges, which corresponds to a limiting cell with a higher overall performance than in Case A. In terms of $V_{\%RMS}$, we notice that the majority of voltage offset from the reference profile occurs in the end-of-discharge region, meaning that pack capacity variations also have an impact here. From Fig. 3c, we can see that positive perturbation Cases B and C belong to a distinct grouping separate from the predominant trend. This distinct grouping consists entirely of points with both high average $\%$-perturbation and a large $\%$-perturbation range. This combination allows them to sustain a higher voltage for a longer duration, which results in a higher $V_{\%RMS}$ than for negative average perturbations, in which the duration over which $V_{\%RMS}$ is calculated will be limited by a low capacity cell. Overall, these results can be interpreted not only as confirming the pack-level effect of cell heterogeneity in design parameter values, but also quantifying the potential prediction error introduced by uncertainty in parameter estimates for modeling and BMS applications.

VII. Conclusion

In this paper, a comprehensive modeling framework for battery packs composed of interconnected LIB cells is presented which is computationally tractable and scalable to a battery pack with numerous cells in series. The framework employs physics-based coupled electrochemical, thermal, and aging models to describe each cell's behavior, and moreover, accounts for thermal interactions in a pack. The cell-level model is further extended to pack-level by expressing the pack-level dynamics in a compact state-space form that can be scaled to larger packs. The pack sensitivity to model parameter perturbation is investigated, revealing the strong impact of cell heterogeneity on pack performance.

[5] $\epsilon_{s,n}$ has a proportional relationship with cell capacity in this modeling framework

VIII. Acknowledgements

The authors acknowledge LG Chem for their financial support of this project and would like to specifically thank Dr. Won Tae Joe and Dr. Yohwan Choi of LG Chem for fostering an excellent working relationship and providing invaluable guidance on our work.

References

[1] A. Allam and S. Onori, "Characterization of aging propagation in lithium-ion cells based on an electrochemical model," in *ACC*, 2016.

[2] T. R. Tanim, M. G. Shirk, R. L. Bewley, E. J. Dufek, and B. Y. Liaw, "Fast charge implications: Pack and cell analysis and comparison," *J. of Power Sources*, 2018.

[3] T. Baumhöfer, M. Brühl, S. Rothgang, and D. U. Sauer, "Production caused variation in capacity aging trend and correlation to initial cell performance," *Journal of Power Sources*, 2014.

[4] A. Cordoba-Arenas, S. Onori, G. Rizzoni, and G. Fan, "Aging propagation in interconnected systems with an application to advanced automotive battery packs," in *7th IFAC Symposium on Advances in Automotive Control*, 2013, pp. 703–716.

[5] A. Pozzi, M. Torchio, and D. M. Raimondo, "Film growth minimization in a li-ion cell: a pseudo two dimensional model-based optimal charging approach," in *2018 ECC*. IEEE, 2018.

[6] F. Altaf, B. Egardt, and L. J. Mårdh, "Load management of modular battery using model predictive control: Thermal and state-of-charge balancing," *IEEE Transactions on Control Systems Technology*, 2016.

[7] A. Cordoba-Arenas, S. Onori, and G. Rizzoni, "A control-oriented lithium-ion battery pack model for plug-in hybrid electric vehicle cycle-life studies and system design with consideration of health management," *Journal of Power Sources*, vol. 279, pp. 791–808, 2015.

[8] D. J. Docimo and H. K. Fathy, "Multivariable state feedback control as a foundation for lithium-ion battery pack charge and capacity balancing," *Journal of The Electrochemical Society*, 2017.

[9] N. Yang, X. Zhang, B. Shang, and G. Li, "Unbalanced discharging and aging due to temperature differences among the cells in a lithium-ion battery pack with parallel combination," *J. of Power Sources*, 2016.

[10] N. Ganesan, S. Basu, K. S. Hariharan, S. M. Kolake, T. Song, T. Yeo, D. K. Sohn, and S. Doo, "Physics based modeling of a series parallel battery pack for asymmetry analysis, predictive control and life extension," *Journal of Power Sources*, vol. 322, pp. 57–67, 2016.

[11] C. D. Rahn and C.-Y. Wang, *Battery systems engineering*. John Wiley & Sons, 2013.

[12] X. Lin, H. E. Perez, S. Mohan, J. B. Siegel, A. G. Stefanopoulou, Y. Ding, and M. P. Castanier, "A lumped-parameter electro-thermal model for cylindrical batteries," *Journal of Power Sources*, 2014.

[13] M. Safari, M. Morcrette, A. Teyssot, and C. Delacourt, "Multimodal physics-based aging model for life prediction of li-ion batteries," *J. of The Electrochemical Society*, 2009.

[14] E. Prada, D. Di Domenico, Y. Creff, J. Bernard, V. Sauvant-Moynot, and F. Huet, "A Simplified Electrochemical and Thermal Aging Model of LiFePO4-Graphite Li-ion Batteries: Power and Capacity Fade Simulations," *Journal of The Electrochemical Society*, 2013.

[15] T. R. Tanim, C. D. Rahn, and C.-Y. Wang, "A temperature dependent, single particle, lithium ion cell model including electrolyte diffusion," *Journal of Dynamic Systems, Measurement, and Control*, 2015.

[16] Y. Ji, Y. Zhang, and C.-Y. Wang, "Li-ion cell operation at low temperatures," *Journal of The Electrochemical Society*, 2013.

[17] L. Valoen and J. Reimers, "Transport properties of lipf6-based li-ion battery electrolytes," *J. of The Electrochemical Society*, 2005.

[18] M. Torchio, L. Magni, R. B. Gopaluni, R. D. Braatz, and D. M. Raimondo, "Lionsimba: A matlab framework based on a finite volume model suitable for li-ion battery design, simulation, and control," *J. of The Electrochemical Society*, 2016.

[19] J. Christensen and J. Newman, "A mathematical model for the lithium-ion negative electrode solid electrolyte interphase," *J. of The Electrochemical Society*, 2004.

[20] A. Allam and S. Onori, "Exploring the dependence of cell aging dynamics on thermal gradient in battery modules: A pde-based time scale separation approach," in *2019 18th ECC*. IEEE, 2019.

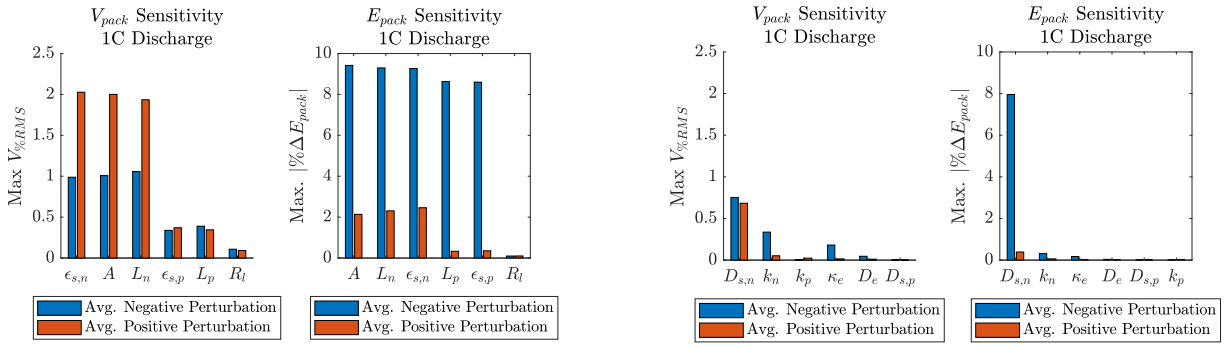

(a) Geometrical parameters ranked by sensitivity

(b) Transport and kinetic parameters ranked by sensitivity

Fig. 2: Pack sensitivity in terms of maximum %RMS change in Pack Voltage and maximum %Δ in Pack Energy resulting from negative/positive average random perturbation of 6-cell series-connected pack compared to unperturbed reference pack during 1C Discharge.

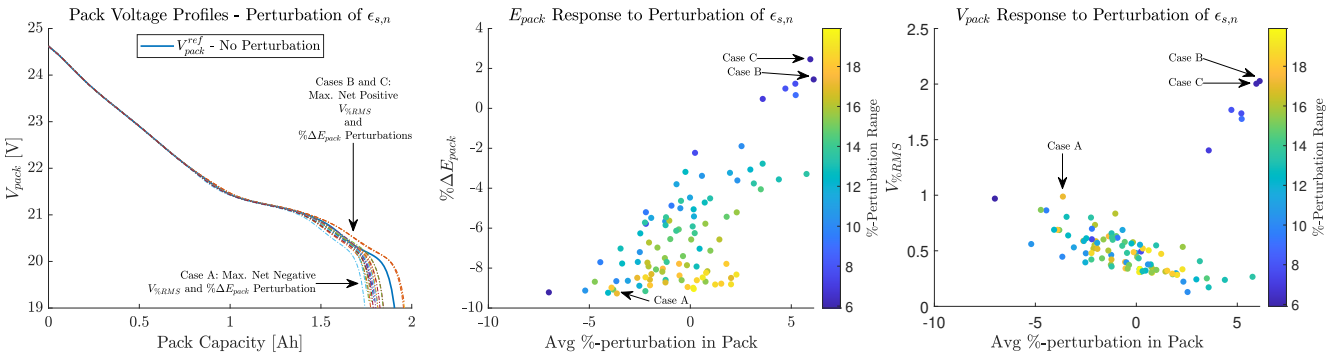

(a) (b) (c)

Fig. 3: a) Pack voltage profiles in response to randomly perturbed anode active material volume fraction $\epsilon_{s,n}$ across pack in comparison with unperturbed reference pack. (b) $\%\Delta E$ sensitivity to $\epsilon_{s,n}$ (c) $V_{\%RMS}$ sensitivity to $\epsilon_{s,n}$. Cases A, B and C are marked for perturbed packs with the maximum magnitude $V_{\%RMS}$ and $\%\Delta E_{pack}$ for negative (A) and positive (B,C) average %-perturbation levels across pack. Case A has the largest magnitude change in both metrics, while Case B and C have maximum magnitude changes in $V_{\%RMS}$ and $\%\Delta E_{pack}$, respectively.

TABLE IV: Nomenclature

$C_{s,j}$	Concentration in solid phase [mol/m^3]	C_e	Concentration in electrolyte phase [mol/m^3]	c_{solv}	Solvent concentration [mol/m^3]
Q	Cell Capacity [Ah]	I_{batt}	Applied current [A]	Φ_e	Electrolyte Potential [V]
$\Phi_{s,n}$	Anode Surface Potential [V]	η_j	Overpotential [V]	$\imath_{0,j}$	Exchange Current Density [A/m^2]
U_j	Open circuit potential (electrode) [V]	V_{oc}	Open circuit potential (cell) [V]	i_s	Side reaction current density [A/m^2]
$D_{s,j}$	Solid phase diffusion [m^2/s]	$R_{s,j}$	Particle radius [m]	$a_{s,j}$	Specific interfacial surface area [m^{-1}]
A	Cell cross sectional area [m^2]	L_j	Domain thickness [m]	F	Faraday's constant [C/mol]
$\epsilon_{e,j}$	Electrolyte Porosity	D_e	Electrolyte phase diffusion [m^2/s]	t_0^+	Transference number
$c_{s,j}^{max}$	Maximum electrode concentration [mol/m^3]	$\kappa_{e,j}$	Electrolyte conductivity [S/m]	κ_D	Diffusional conductivity [S/m]
k_j	Intercalation rate constant [m$^{2.5}$/s-mol$^{0.5}$]	R_l	Lumped contact resistance [Ω]	R_g	Universal gas constant [J/mol-K]
$\epsilon_{s,j}$	Active volume fraction of solid phase	$\epsilon_{f,j}$	Active volume fraction of filler/binder	D_{solv}	Solvent diffusion coefficient in SEI layer [m^2/s]
ϵ_{sei}	SEI Layer porosity	ρ_{sei}	SEI layer density [kg/m^3]	κ_{sei}	SEI layer ionic conductivity [S/m]
c_{solv}	Solvent concentration [mol/m^3]	M_{sei}	Molar mass of SEI layer [kg/mol]	U_s	Solvent reduction potential [V]
k_f	Solvent Reduction rate constant [mol$^-$2s$^-$1]	β	Side Reaction charge transfer coefficient	C_s	Heat Capacity of cell surface [J/K]
C_c	Heat Capacity of cell core [J/K]	R_c	Conductive resistance - core/surface [K/W]	R_u	Convective resistance - surface/surroundings [K/W]
R_m	Cell-to-cell heat transfer resistance [K/W]	T_{amb}	Ambient temperature [K]	$N_{r,j}$	Number of radial discretization points
$N_{x,j}$	Number of cartesian discretization points	N_{el}	Total number of electrolyte discretization points	N_{sei}	Number of SEI layer discretization points